

# 1 An Antioxidant Enzyme Therapeutic for COVID-19

2 Meng Qin<sup>1\*</sup>, Zheng Cao<sup>3\*</sup>, Jing Wen<sup>3\*</sup>, Qingsong Yu<sup>1</sup>, Chaoyong Liu<sup>1</sup>, Fang Wang<sup>1</sup>, Fengmei  
3 Yang<sup>2</sup>, Yanyan Li<sup>2</sup>, Gregory Fishbein<sup>3</sup>, Sen Yan<sup>4</sup>, Bin Xu<sup>3</sup>, Yi Hou<sup>1</sup>, Zhenbo Ning<sup>1</sup>, Kaili Nie<sup>1</sup>,  
4 Ni Jiang<sup>1</sup>, Zhen Liu<sup>1</sup>, Jun Wu<sup>1</sup>, Yanting Yu<sup>1</sup>, Heng Li<sup>2</sup>, Huiwen Zheng<sup>2</sup>, Jing Li<sup>2</sup>, Weihua Jin<sup>2</sup>,  
5 Sheng Pan<sup>5</sup>, Shuai Wang<sup>5</sup>, Jianfeng Chen<sup>1‡</sup>, Zhihua Gan<sup>1‡</sup>, Zhanlong He<sup>2‡</sup> and Yunfeng Lu<sup>3‡</sup>

6

7 1. State Key Laboratory of Organic-inorganic Composites, Beijing Advanced Innovation Center  
8 for Soft Matter Science and Engineering, College of Life Science and Technology, Beijing  
9 University of Chemical Technology, Beijing, 100029, China.

10 2. Institute of Medical Biology, Chinese Academy of Medical Sciences, Peking Union Medical  
11 College, Yunnan Key Laboratory of Vaccine Research Development on Severe Infectious Disease,  
12 Kunming, 650118, China.

13 3. Department of Chemical and Molecular Engineering, Microbiology, Immunology and  
14 Molecular Genetics, and the David Geffen School of Medicine, University of California, Los  
15 Angeles, CA 90095, U.S.A.

16 4. Guangdong-Hongkong-Macau Institute of CNS Regeneration, Jinan University, Guangdong,  
17 China.

18 5. Vivibaba, Inc, 570 Westwood Plaza, University of California, Los Angeles, CA 90095.

19 \*These authors contributed equally to this work.

20 ‡Corresponding author. Email addresses: (J. Chen) [chenjf@mail.buct.edu.cn](mailto:chenjf@mail.buct.edu.cn); (Z. Gan)  
21 [zhgan@mail.buct.edu.cn](mailto:zhgan@mail.buct.edu.cn); (Z. He) [hzl612@126.com](mailto:hzl612@126.com); (Y. Lu) [luucla@ucla.edu](mailto:luucla@ucla.edu)

22

23 The COVID-19 pandemic has taken a significant toll on people worldwide, and there  
24 are currently no specific antivirus drugs or vaccines. We report herein a therapeutic based  
25 on catalase, an antioxidant enzyme that can effectively breakdown hydrogen peroxide and  
26 minimize the downstream reactive oxygen species, which are excessively produced resulting  
27 from the infection and inflammatory process. Catalase assists to regulate production of  
28 cytokines, protect oxidative injury, and repress replication of SARS-CoV-2, as demonstrated  
29 in human leukocytes and alveolar epithelial cells, and *rhesus macaques*, without noticeable  
30 toxicity. Such a therapeutic can be readily manufactured at low cost as a potential treatment  
31 for COVID-19.

32 The severe acute respiratory syndrome coronavirus 2 (SARS-CoV-2) has resulted in over  
33 ten million COVID-19 cases globally. Broad-spectrum antiviral drugs (e.g., nucleoside analogues  
34 and HIV-protease inhibitors) are being utilized to attenuate the infection. However, current  
35 management is supportive, and without specific antivirus drugs or vaccine against COVID-19(1).  
36 While the pathogenesis of COVID-19 remains elusive, accumulating evidence suggests that a  
37 subgroup of patients with severe COVID-19 might have cytokine storm syndrome(2, 3). Cytokine  
38 storm is a serious immune dysregulation resultant from overproduction of cytokines, which often  
39 occurs during virus infection(4), organ transplant(5), immunotherapy(6), and autoimmune  
40 diseases(7), and may result in death if untreated(8). Treatment of hyperinflammation and  
41 immunosuppression are highly recommended to address the immediate need to reduce mortality(2).  
42 Current immunosuppression options include steroids(9), intravenous immunoglobulin(10),

43 selective cytokine blockade (e.g., anakinra(11) or tocilizumab(12)), and Janus kinase  
44 inhibition(13).

45 In light of the findings that elevated levels of reactive oxygen species (ROS) is strongly  
46 correlated with inflammation,(14) oxidative injury,(15) as well as viral infection and  
47 replication(16–18), we speculate that regulating the ROS level in COVID-19 patients could be  
48 effective for the treatment of hyperinflammation, protection of tissues from oxidative injury, and  
49 repression of viral replication. As illustrated in **Scheme 1A**, after infection of SARS-CoV-2,  
50 leukocytes are attracted to affected sites releasing cytokines and ROS. An increasing ROS level  
51 promotes viral replication, causes oxidative injury, and induces cell apoptosis through DNA  
52 damage, lipid peroxidation and protein oxidation, which further exacerbates the immune response.  
53 As a result, an increasing number of leukocytes are recruited, further releasing ROS and cytokines,  
54 resulting in hyperinflammation and cytokine storm syndrome.

55 ROS are a class of partially reduced metabolites of oxygen that possess strong oxidizing  
56 capability, which are generated as byproducts of cellular metabolism through the electron transport  
57 chains in mitochondria and cytochrome P450(19). The other major source are oxidases(15) (e.g.,  
58 NAPDH oxidase), which are ubiquitously present in a variety of cells, particularly phagocytes and  
59 endothelial cells. As shown in **Scheme 1B**, partial reduction of O<sub>2</sub> in these processes generates  
60 superoxide anions (·O<sub>2</sub><sup>-</sup>), which are rapidly converted to hydrogen peroxide (H<sub>2</sub>O<sub>2</sub>) mediated by  
61 superoxide dismutase (SOD). H<sub>2</sub>O<sub>2</sub> may subsequently react forming hydroxyls (OH· and OH<sup>-</sup>)  
62 through the Fenton reaction, HOCl through myeloperoxidase (MPO), H<sub>2</sub>O through  
63 glutathione/glutathione peroxidase (GSH/GPX), and H<sub>2</sub>O/O<sub>2</sub> through catalase (CAT),  
64 respectively(19). Since ·O<sub>2</sub><sup>-</sup> possesses a short half-life (~10<sup>-6</sup> s)(20), it is rapidly converted to H<sub>2</sub>O<sub>2</sub>,  
65 which is chemically stable and able to cross cell membranes and diffuse in tissues. Under a  
66 pathological condition, where ROS are excessively produced but antioxidant enzymes are  
67 insufficiently presented, H<sub>2</sub>O<sub>2</sub> may accumulate locally or systematically(21), which oxidizes  
68 proteins with sulfur-containing residues (cysteine and methionine) and reacts with transition  
69 metals (e.g., iron), generating downstream ROS that are highly active(22, 23). In the context of  
70 reaction pathways and kinetics, eliminating the excessive H<sub>2</sub>O<sub>2</sub> is critical to minimize the  
71 formation of downstream ROS, prevent oxidative injury, and avoid immunopathogenesis.

72 Catalase, the most abundant antioxidant enzyme ubiquitously present in the liver,  
73 erythrocytes and alveolar epithelial cells, is the most effective catalyst for the decomposition of  
74 H<sub>2</sub>O<sub>2</sub>(24). One catalase molecule can breakdown 10<sup>7</sup> H<sub>2</sub>O<sub>2</sub> molecules in 1 s with an extremely  
75 high turnover number of 10<sup>7</sup> s<sup>-1</sup>; however, catalase generally exhibits poor stability and a short  
76 plasma half-life(25). To explore its therapeutic use, we encapsulated catalase with a thin shell of  
77 polymer through *in situ* polymerization(26, 27). As illustrated in **Scheme 1C**, 2-  
78 methacryloyloxyethyl phosphorylcholine (MPC), N-(3-aminopropyl) methacrylamide  
79 hydrochloride (APM), and N,N'-methylenebisacrylamide (BIS) are used as the monomers and  
80 crosslinker. These molecules are enriched around the catalase molecules through noncovalent  
81 interactions; subsequent polymerization grows a thin polymeric shell around individual catalase  
82 molecules, forming nanocapsules denoted as n(CAT). The thin shell protects the enzyme, while  
83 allowing H<sub>2</sub>O<sub>2</sub> to rapidly transport through, endowing n(CAT) with high enzyme activity,  
84 augmented stability, and improved plasma half-life.

85 As shown in **Fig. 1A, B**, n(CAT) shows a size distribution centered at 25 nm and a zeta  
86 potential of 1.5 mV, in comparison with those of native catalase (10 nm and - 4.0 mV); TEM image  
87 confirms that n(CAT) has an average size of 20~30 nm (**Fig. 1C**). Compared with native catalase,  
88 n(CAT) exhibits a similar enzyme activity (**fig. S1A**), yet with significantly improved enzyme  
89 stability. As shown in **Fig. 1E, F**, n(CAT) and native catalase retain 90% and 52% of the activity  
90 after incubation in PBS at 37 °C for 24 h, respectively, indicating improved thermal stability. After  
91 incubation in PBS with 50 µg/mL trypsin at 37 °C for 2 h, n(CAT) and native catalase retain 87%  
92 and 30% of the activity, respectively, suggesting improved protease stability. In addition, n(CAT)  
93 in solution retains 100% of the activity after storage at 4 °C and 25 °C for 3 mo. (**fig. S1B**); after  
94 freeze drying, n(CAT) retains more than 90% of the activity (**fig. S1C**). Such characteristics are  
95 critical for the transport and distribution of n(CAT).

96 The ability of n(CAT) to protect lung tissues from oxidative injury was examined in human  
97 pulmonary alveolar epithelial cells (HPAEpiC). We first investigated the cytotoxicity of n(CAT)  
98 by culturing HPAEpiC with different concentrations of n(CAT) (**fig. S2A**). The cells with n(CAT)  
99 exhibit similar or higher cell viability than the control cells, indicating that n(CAT) does not show  
100 any noticeable cytotoxicity to HPAEpiC. The higher cell viability observed is possibly attributable  
101 to the ability of n(CAT) to remove H<sub>2</sub>O<sub>2</sub> produced in the cultures. To examine the protective effect,  
102 HPAEpiC were cultured with 20 µg/mL of n(CAT) for 12 h, after which 1,000 µM H<sub>2</sub>O<sub>2</sub> was  
103 added to the media and cultured for 24 h (**Fig. 1F**). The cells without n(CAT) show a cell viability  
104 of 63%, while the cells with n(CAT) retain 100% of the cell viability, demonstrating an ability to  
105 protect the cells from oxidative injury. In addition, HPAEpiC were incubated with 1000 µM H<sub>2</sub>O<sub>2</sub>  
106 for 24 h to induce cell injury, after which the injured cells were incubated with 20 µg/mL of n(CAT)  
107 for 12 h (**Fig. 1G**). Culturing the injured cells with n(CAT) increases the cell viability from 50%  
108 to 73%, indicating an ability of n(CAT) to resuscitate injured cells. Similar protective and  
109 resuscitative effects were also observed with lower n(CAT) concentrations (**fig. S2B, C**).

110 Hyperinflammatory response induced by SARS-CoV-2 is a major cause of disease severity  
111 and death in patients with COVID-19. The infection and the destruction of lung cells trigger a  
112 local immune response, recruiting leukocytes to affected sites(28). Unrestrained inflammatory  
113 cell infiltration, however, results in excessive secretion of proteases and ROS. In addition to the  
114 damage resulting from the virus itself, dysfunctional immune response results in diffusive alveolar  
115 damage, including desquamation of alveolar cells, hyaline membrane formation, and pulmonary  
116 oedema(29). Overproduction of pro-inflammation cytokines is commonly observed in COVID-  
117 19 patients, in whom the severity is strongly correlated to the level of cytokines, such as tumor  
118 necrosis factor  $\alpha$  (TNF- $\alpha$ ) and interleukin 10 (IL-10)(30, 31). Regulating the production of  
119 cytokines, in this context, is critical to reinstate immune homeostasis, and anti-cytokine therapy  
120 (e.g., TNF- $\alpha$  antagonist) has been suggested for alleviation of hyperinflammation in severe  
121 cases(32).

122 In light of these findings, the ability of n(CAT) to regulate cytokine production was studied  
123 in human leukocytes (white blood cells, WBC). Leukocytes were cultured with  
124 lipopolysaccharides (LPS, a bacterial endotoxin that activates leukocytes) with and without  
125 n(CAT). **Fig. 1H, I** show the concentration of TNF $\alpha$  and IL-10 in the culture media. Culturing  
126 the leukocytes with LPS without n(CAT) significantly increases the production of TNF- $\alpha$  and IL-  
127 10 ( $P$  value 0.0001). Moreover, the cultures with n(CAT) show dramatically lower concentrations

128 of TNF- $\alpha$  and IL-10 ( $P$  value 0.01 to 0.001), that are comparable with those of the control cells  
129 (resting leukocytes). This *ex vivo* study suggests that n(CAT) can downregulate the production of  
130 TNF- $\alpha$  and IL-10 by activated leukocytes, indicating a potential use of n(CAT) as an  
131 immunoregulator for hyperinflammation.

132 To further elucidate the immunoregulatory effect, leukocytes were cultured with injured  
133 HPAEpiC, of which cell injury was induced by H<sub>2</sub>O<sub>2</sub> (Control #1, cell viability 85%). As shown  
134 in **Fig. 1J**, culturing the cells with leukocytes reduces the viability to 71%. Furthermore, adding  
135 8, 16, and 40  $\mu$ g/mL n(CAT) increases the viability to 82, 89, and 91%, respectively, which are  
136 comparable to those of Control #2 (leukocytes with untreated-HPAEpiC, 91% cell viability). This  
137 finding indicates that n(CAT) can not only protect, but also resuscitate, the injured alveolar cells,  
138 which is consistent with the observation presented in **Fig. 1G**. Furthermore, HPAEpiC was  
139 cultured with leukocytes activated by LPS. As shown in **Fig. 1K**, HPAEpiC (Blank) and  
140 HPAEpiC with LPS (Control #3) exhibit a similar cell viability, while HPAEpiC with LPS-  
141 activated leukocytes show a dramatically reduced cell viability of 67%. Moreover, adding 8, 16,  
142 and 40  $\mu$ g/mL n(CAT) increases the cell viability to 78, 88, and 91%, respectively, which are  
143 comparable with those of Control #4 (un-activated leukocytes and HPAEpiC, cell viability 91%).  
144 This study suggests that n(CAT) can also protect healthy alveolar cells from injury by activated  
145 leukocytes, indicating an anti-inflammatory effect.

146 For therapeutic use, we first investigated the pharmacokinetics and biodistribution of  
147 n(CAT) in mice. For intravenous administration, BALB/c mice were administered 20 mg/kg of  
148 native catalase or n(CAT). **Fig. 2A** shows the biodistribution 6 h and 24 h post-injection;  
149 accumulation of n(CAT) is observed in the liver, kidney, lung, and lymph nodes, of which the  
150 average radiance is shown in **Fig. 2B**. **Fig. 2C** presents the pharmacokinetics, indicating that  
151 n(CAT) has a significantly longer circulation time than the native catalase. Based on the one-  
152 compartment model, n(CAT) exhibits a serum half-life of 8.9 h, which is 16.8-fold longer than the  
153 native CAT (0.5 h). Further analysis of the drug exposure time through the area under the curve  
154 (AUC) indicates that the mice that received n(CAT) had a significantly increased body exposure  
155 to catalase compared to the mice with native CAT (~ 2.5-fold increase) (**Fig. 2D**). The following  
156 were all within the normal ranges: the plasma levels of alanine aminotransferase, aspartate  
157 aminotransferase, and alkaline phosphatase (**fig. S3A**); the levels of urea and uric acid (**fig. S3B**);  
158 the total white blood cell (WBC) count; and the counts of lymphocytes, monocytes, and  
159 granulocytes (**fig. S3C**). Furthermore, H&E stained sections of the main organs do not show any  
160 noticeable tissue damage (**fig. S4**).

161 For intratracheal nebulization, BALB/c mice were administered 2.5 mg/kg of native CAT  
162 or n(CAT) labeled with Alexa-Fluor-750. The mice receiving native catalase show fluorescent  
163 signal in the lung after 6 h, the intensity of which decreases significantly after 48 h. The mice  
164 receiving n(CAT) exhibit significantly higher fluorescent intensity after 6 h and 48 h (**Fig. 2E**),  
165 which is confirmed by their fluorescent intensity plot after 48 h (**Fig. 2F**). Except the lung, other  
166 organs (heart, liver, spleen, and kidney) after 48 h show negligible fluorescent signal, indicating  
167 that the as-administered n(CAT) was mainly retained within the lung. H&E stained sections of  
168 the main organs do not show any noticeable tissue damage (**fig. S5**).

169 The ability of n(CAT) to repress the replication of SARS-CoV-2 was examined in *rhesus*  
170 *macaques*. As illustrated in **Fig. 3A**, at day 0, all of the animals were inoculated with SARS-CoV-

171 2 through the intranasal route. For the control group (C1, C2), two animals received 10 mL PBS  
172 though inhalation at day 2, 4, and 6, respectively. For the nebulization group, three animals (N1,  
173 N2, N3) received 5 mg of n(CAT) (10 mL) through inhalation at day 2, 4, and 6. For the  
174 intravenous group, two animals (I1, I2) received 10 mL PBS though inhalation and 5 mg/kg of  
175 n(CAT) intravenously at day 2, 4, and 6. Except N3 (sacrificed at day 21), the other animals were  
176 sacrificed at day 7.

177 **Fig. 3B** shows the viral loads in nasal swabs for the control and nebulized group. N1  
178 exhibits a viral load that is similar to C1 and C2 at day 1 and 2, after which the viral load rapidly  
179 decreases and becomes significantly lower than the control group. N3 shows a similar viral load  
180 to the control group at day 1, after which the viral load remains significantly lower than the control  
181 group. It is worth noting that the viral load of N3 at day 2 is lower than the control group.  
182 Nevertheless, the oral swabs confirmed that N3 was successfully infected, indicating an individual  
183 difference (**fig. S6**). N2 shows similar viral loads to the control group from day 1 to 7. **Fig. 3C**  
184 shows viral loads in the nasal swabs for the control and intravenous group. I1 exhibits a similar  
185 viral load to the control group at day 1 and 2, after which the viral load rapidly decreases and  
186 remains significantly lower than the control group. I2 also shows a similar viral load to the control  
187 group at day 1, after which the viral load remains significantly lower than the control group.  
188 Similarly, I2 shows a lower viral load than the control group, yet the oral swabs confirmed its  
189 active infection. **Fig. 3E-F** presents the viral RNA copy numbers in 100 mg of the organs,  
190 including lung, trachea, neck lymph node (LN), and lung LN. N1 shows significantly lower viral  
191 loads than the control group; whereas, N2 exhibits similar viral loads to the control group, which  
192 is consistent with the nasal-swab results. I1 and I2 show significantly lower viral loads than the  
193 control group, which is consistent with the nasal-swab results. No virus is detected from the organs  
194 of N3 (**fig. S7**). **Fig. 3D** shows the bodyweight change of the animals, suggesting that the  
195 experiment groups have less weight lost. These results confirm the ability of n(CAT) to repress  
196 the replication of SARS-CoV-2 in *rhesus macaques*.

197 **Fig. 4A-F** shows the liver and renal functions of the control and experimental group, which  
198 exhibit similar levels of alanine aminotransferase, aminotransferase aspartate aminotransferase,  
199 alkaline phosphatase, albumin, uric acid, creatine, and blood urea nitrogen, indicating that  
200 intravenous administration of 5 mg/kg of n(CAT) did not cause any noticeable liver or renal  
201 toxicity. Meanwhile, all of the groups show similar blood routine and other indexes for liver  
202 function (**fig. S8**). Similar results were also observed in healthy *rhesus macaques* inhaling 2.0  
203 mg/kg (**fig. S9**) n(CAT) per day for 7 d, suggesting that n(CAT) does not cause noticeable liver or  
204 kidney toxicity.

205 **Fig. 4G** presents representative H&E sections of kidneys (a, b) and liver (c, d) from animals  
206 in the control (a, c) and inhaled group (b, d). The kidneys show neither evidence of interstitial  
207 nephritis nor acute tubular injury; the livers exhibit neither steatosis, hepatocyte necrosis,  
208 inflammation, cholestasis, nor bile duct injury. Histologic sections of lung tissues in both the  
209 control and inhaled groups exhibit unremarkable alveolar architecture, with no evidence of acute  
210 lung injury in the form of hyaline membranes, intra-alveolar fibrin, organizing pneumonia, or  
211 reactive pneumocyte hyperplasia. The airway epithelium is unremarkable. Vascular  
212 compartments are free of thrombi (**fig. S10**). There is no evidence of eosinophilia or vasculitis,  
213 and no viral cytopathic effect is identified. The H&E staining of other major organs also shows  
214 no tissue injury for both the control and inhaled group (**fig. S11**), confirming the biosafety of

215 n(CAT) administered through intravenous injection or inhalation. In addition, **Fig. 4H** also  
216 presents a representative H&E section (a) and immunohistochemistry for SARS-CoV-2  
217 nucleocapsid protein (b) of the lung LN in one animal from the control group (C1). Reactive  
218 follicular hyperplasia could be observed in the H&E section, and scattered positive mononuclear  
219 cells (black arrows) indicate the SARS-CoV-2 infection in the lymph node.

220 The action mechanism of n(CAT) is unclear. In addition to being a weapon against  
221 pathogens, ROS also serve as signaling molecules in numerous physiological processes.(33) For  
222 example, it has been documented that H<sub>2</sub>O<sub>2</sub> generation after wounding is required for the  
223 recruitment of leukocytes to the wound(34), and ROS is necessary for the release of pro-  
224 inflammatory cytokines to modulate an appropriate immune response(22). Eliminating the H<sub>2</sub>O<sub>2</sub>  
225 excessively produced during inflammation also minimizes the downstream ROS, which assists to  
226 downregulate production of cytokines, mitigate recruitment of excessive leukocytes, and repress  
227 replication of the viruses. It is also worth noting that immunosuppressive steroids, such as  
228 prednisone and dexamethasone, are proven to be effective for treatment of hyperinflammation in  
229 severe COVID-19 patients(9). Glucocorticoids constitute powerful, broad-spectrum anti-  
230 inflammatory agents that regulate cytokine production, but their utilization is complicated by an  
231 equally broad range of adverse effects(35, 36). For instance, in a retrospective study of 539  
232 patients with SARS who received corticosteroid treatment, one-fourth of the patients developed  
233 osteonecrosis of the femoral head(37). We speculate that n(CAT) could also regulate cytokine  
234 production, but through a different pathway – reinstating immune homeostasis through eliminating  
235 excessively produced ROS.

236 In conclusion, we have shown the anti-inflammatory effect and ability of catalase to  
237 regulate cytokine production in leukocytes, protect alveolar cells from oxidative injury, and repress  
238 the replication of SARS-CoV-2 in *rhesus macaques* without noticeable toxicity. Moreover, it is  
239 worth noting that catalase is safe and commonly used as a food additive and dietary supplement,  
240 and that pilot-scale manufacturing of n(CAT) has been successfully demonstrated. In contrast to  
241 the current focus on vaccines and antiviral drugs, this may provide an effective therapeutic solution  
242 for the pandemic, as well as treatment of hyperinflammation in general.

## 243 References

- 244 1. C. Scavone *et al.*, Current pharmacological treatments for COVID-19: What's next? *Br. J. Pharmacol.* (2020), doi:10.1111/bph.15072.
- 245 2. P. Mehta *et al.*, COVID-19: consider cytokine storm syndromes and immunosuppression. *Lancet.* **395**, 1033–1034 (2020).
- 246 3. C. Huang *et al.*, Clinical features of patients infected with 2019 novel coronavirus in Wuhan, China. *Lancet.* **395**, 497–506 (2020).
- 247 4. Q. Liu, Y. Zhou, Z. Yang, The cytokine storm of severe influenza and development of immunomodulatory therapy. *Cell Mol Immunol.* **13**, 3–10 (2016).
- 248 5. G. R. Hill, J. L. Ferrara, The primacy of the gastrointestinal tract as a target organ of acute graft-versus-host disease: rationale for the use of cytokine shields in allogeneic bone marrow transplantation. *Blood.* **95**, 2754–2759 (2000).
- 249 6. R. M. Sterner *et al.*, GM-CSF inhibition reduces cytokine release syndrome and neuroinflammation but enhances CAR-T cell function in xenografts. *Blood.* **133**, 697–709 (2019).

259 7. J. J. O'Shea, A. Ma, P. Lipsky, Cytokines and autoimmunity. *Nat. Rev. Immunol.* **2**, 37–45  
260 (2002).

261 8. J. R. Tisoncik *et al.*, Into the eye of the cytokine storm. *Microbiol. Mol. Biol. Rev.* **76**, 16–  
262 32 (2012).

263 9. K. Kupferschmidt, A cheap steroid is the first drug shown to reduce death in COVID-19  
264 patients. *Science* (2020), doi:10.1126/science.abd3683.

265 10. A. A. Nguyen *et al.*, Immunoglobulins in the treatment of COVID-19 infection: Proceed  
266 with caution! *Clin. Immunol.* **216**, 108459 (2020).

267 11. T. Huet *et al.*, Anakinra for severe forms of COVID-19: a cohort study. *The Lancet  
268 Rheumatology* (2020), doi:10.1016/S2665-9913(20)30164-8.

269 12. G. Guaraldi *et al.*, Tocilizumab in patients with severe COVID-19: a retrospective cohort  
270 study. *The Lancet Rheumatology* (2020), doi:10.1016/S2665-9913(20)30173-9.

271 13. F. La Rosée *et al.*, The Janus kinase 1/2 inhibitor ruxolitinib in COVID-19 with severe  
272 systemic hyperinflammation. *Leukemia* (2020), doi:10.1038/s41375-020-0891-0.

273 14. M. Mittal, M. R. Siddiqui, K. Tran, S. P. Reddy, A. B. Malik, Reactive oxygen species in  
274 inflammation and tissue injury. *Antioxid. Redox Signal.* **20**, 1126–1167 (2014).

275 15. M. Schieber, N. S. Chandel, ROS function in redox signaling and oxidative stress. *Curr.  
276 Biol.* **24**, R453–62 (2014).

277 16. D. Amatore *et al.*, Influenza virus replication in lung epithelial cells depends on redox-  
278 sensitive pathways activated by NOX4-derived ROS. *Cell Microbiol.* **17**, 131–145 (2015).

279 17. R. Vlahos *et al.*, Inhibition of Nox2 oxidase activity ameliorates influenza A virus-induced  
280 lung inflammation. *PLoS Pathog.* **7**, e1001271 (2011).

281 18. M. Sebastian, O. Chastel, B. de Thoisy, M. Eens, D. Costantini, Oxidative stress favours  
282 herpes virus infection in vertebrates: a meta-analysis. *Curr. Zool.* **62**, 325–332 (2016).

283 19. P. Patlevič, J. Vašková, P. Švorc, L. Vaško, P. Švorc, Reactive oxygen species and  
284 antioxidant defense in human gastrointestinal diseases. *Integrative Medicine Research.* **5**,  
285 250–258 (2016).

286 20. A. Phaniendra, D. B. Jestadi, L. Periyasamy, Free radicals: properties, sources, targets, and  
287 their implication in various diseases. *Indian J. Clin. Biochem.* **30**, 11–26 (2015).

288 21. E. Majewska *et al.*, Elevated exhalation of hydrogen peroxide and thiobarbituric acid  
289 reactive substances in patients with community acquired pneumonia. *Respir. Med.* **98**,  
290 669–676 (2004).

291 22. C. Nathan, A. Cunningham-Bussel, Beyond oxidative stress: an immunologist's guide to  
292 reactive oxygen species. *Nat. Rev. Immunol.* **13**, 349–361 (2013).

293 23. I. B. Slimen *et al.*, Reactive oxygen species, heat stress and oxidative-induced  
294 mitochondrial damage. A review. *Int. J. Hyperthermia.* **30**, 513–523 (2014).

295 24. M. Nishikawa, M. Hashida, Y. Takakura, Catalase delivery for inhibiting ROS-mediated  
296 tissue injury and tumor metastasis. *Adv. Drug Deliv. Rev.* **61**, 319–326 (2009).

297 25. X. Shi *et al.*, PEGylated human catalase elicits potent therapeutic effects on H1N1  
298 influenza-induced pneumonia in mice. *Appl. Microbiol. Biotechnol.* **97**, 10025–10033  
299 (2013).

300 26. S. Liang *et al.*, Phosphorylcholine polymer nanocapsules prolong the circulation time and  
301 reduce the immunogenicity of therapeutic proteins. *Nano Res.* **9**, 1022–1031 (2016).

302 27. M. Yan *et al.*, A novel intracellular protein delivery platform based on single-protein  
303 nanocapsules SUPPLEMENTARY INFORMATION. *Nat. Nanotechnol.* **5**, 48–53 (2010).

304 28. M. Merad, J. C. Martin, Pathological inflammation in patients with COVID-19: a key role

305 for monocytes and macrophages. *Nat. Rev. Immunol.* **20**, 355–362 (2020).

306 29. M. Z. Tay, C. M. Poh, L. Rénia, P. A. MacAry, L. F. P. Ng, The trinity of COVID-19:  
307 immunity, inflammation and intervention. *Nat. Rev. Immunol.* **20**, 363–374 (2020).

308 30. J. Gong *et al.*, Correlation Analysis Between Disease Severity and Inflammation-related  
309 Parameters in Patients with COVID-19 Pneumonia. *medRxiv* (2020),  
310 doi:10.1101/2020.02.25.20025643.

311 31. N. Roshanravan, F. Seif, A. Ostadrahimi, M. Pouraghaei, S. Ghaffari, Targeting Cytokine  
312 Storm to Manage Patients with COVID-19: A Mini-Review. *Arch Med Res* (2020),  
313 doi:10.1016/j.arcmed.2020.06.012.

314 32. A. Marchesoni *et al.*, TNF-alpha antagonist survival rate in a cohort of rheumatoid arthritis  
315 patients observed under conditions of standard clinical practice. *Ann. N. Y. Acad. Sci.* **1173**,  
316 837–846 (2009).

317 33. H. Sies, D. P. Jones, Reactive oxygen species (ROS) as pleiotropic physiological signalling  
318 agents. *Nat. Rev. Mol. Cell Biol.* (2020), doi:10.1038/s41580-020-0230-3.

319 34. P. Niethammer, C. Grabher, A. T. Look, T. J. Mitchison, A tissue-scale gradient of  
320 hydrogen peroxide mediates rapid wound detection in zebrafish. *Nature*. **459**, 996–999  
321 (2009).

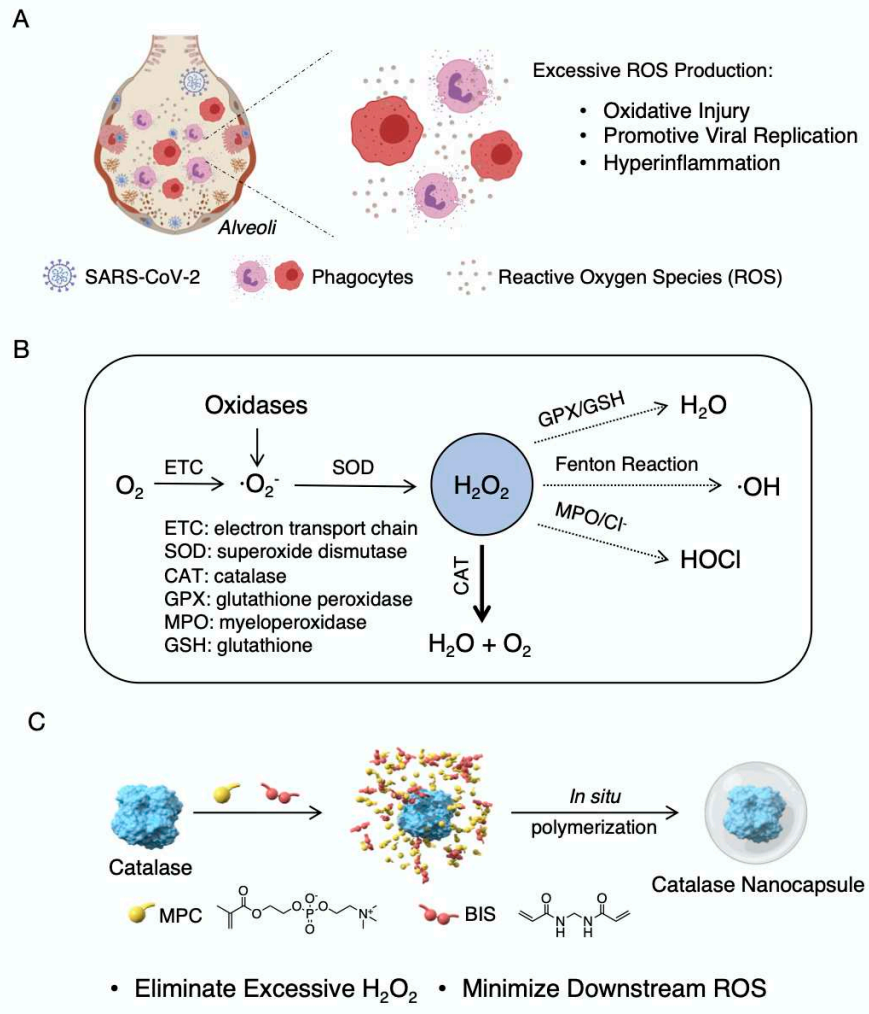
322 35. R. S. Hardy, K. Raza, M. S. Cooper, Therapeutic glucocorticoids: mechanisms of actions  
323 in rheumatic diseases. *Nat. Rev. Rheumatol.* **16**, 133–144 (2020).

324 36. C. Tang, Y. Wang, H. Lv, Z. Guan, J. Gu, Caution against corticosteroid-based COVID-19  
325 treatment. *Lancet*. **395**, 1759–1760 (2020).

326 37. K. J. Guo *et al.*, The influence of age, gender and treatment with steroids on the incidence  
327 of osteonecrosis of the femoral head during the management of severe acute respiratory  
328 syndrome: a retrospective study. *Bone Joint J.* **96-B**, 259–262 (2014).

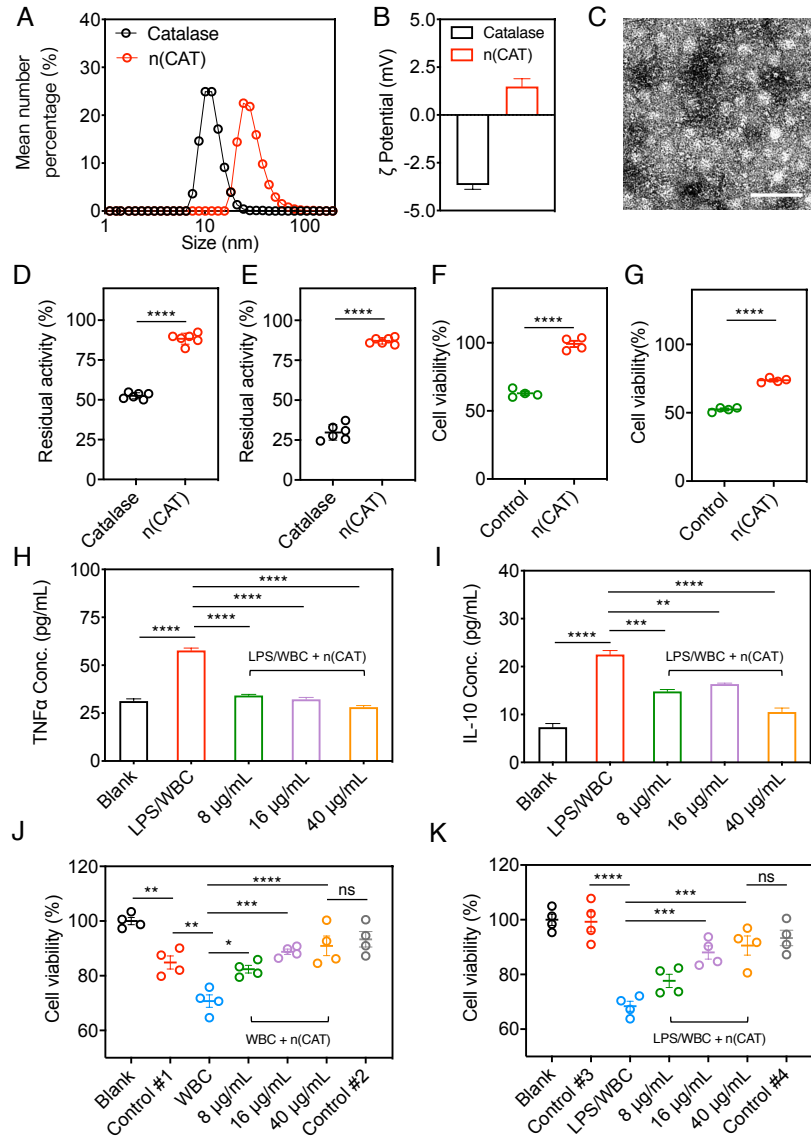
329

330



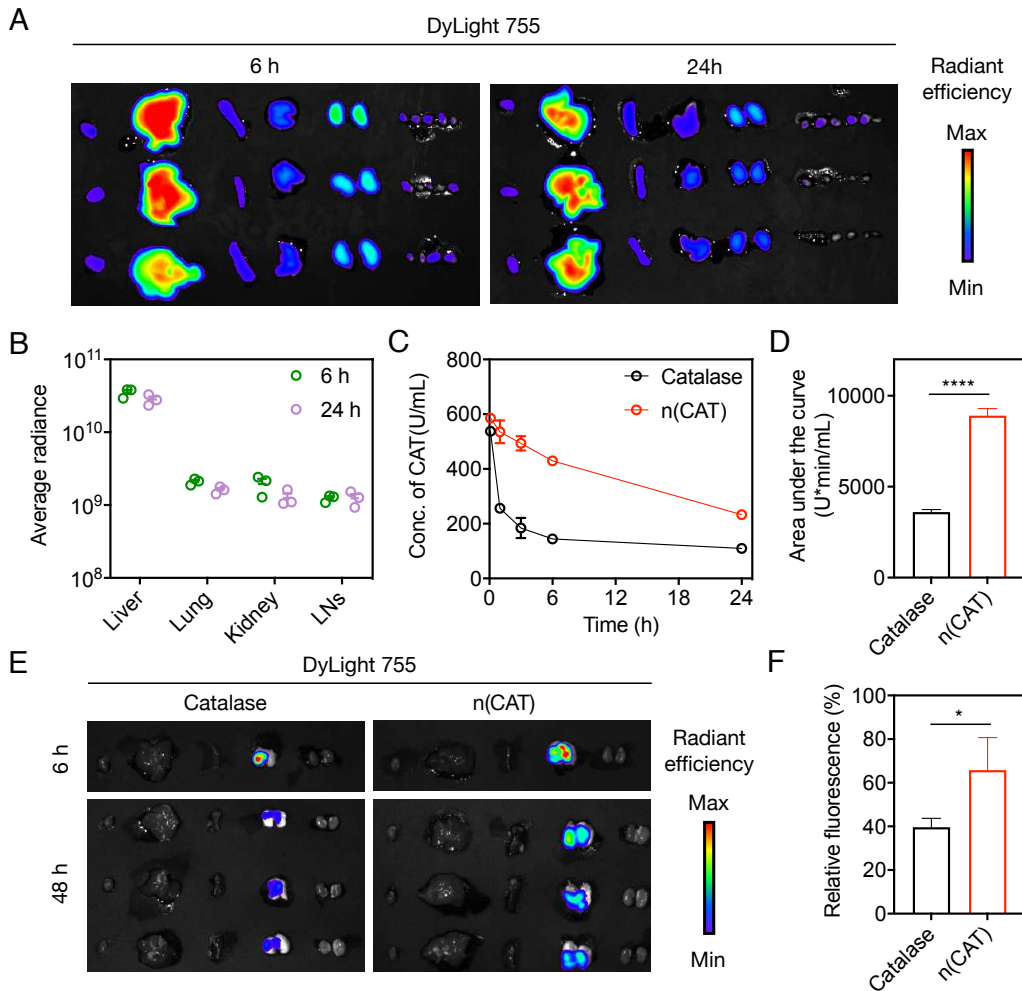
331

332 **Scheme 1. Proposed mechanism of action and synthesis of catalase nanocapsules.** (A) A  
333 schematic illustrating that an elevated level of ROS causes oxidative injury, promotes viral  
334 replication, and triggers cytokine storm syndrome in COVID-19 patients. (B) The reaction  
335 pathways of ROS, suggesting that eliminating  $H_2O_2$  is the key to minimizing the formation of  
336 downstream ROS. (C) The synthesis of catalase nanocapsules by *in situ* polymerization of MPC  
337 and BIS around individual catalase molecules exhibiting improved stability and circulation half-  
338 life.  
339



340

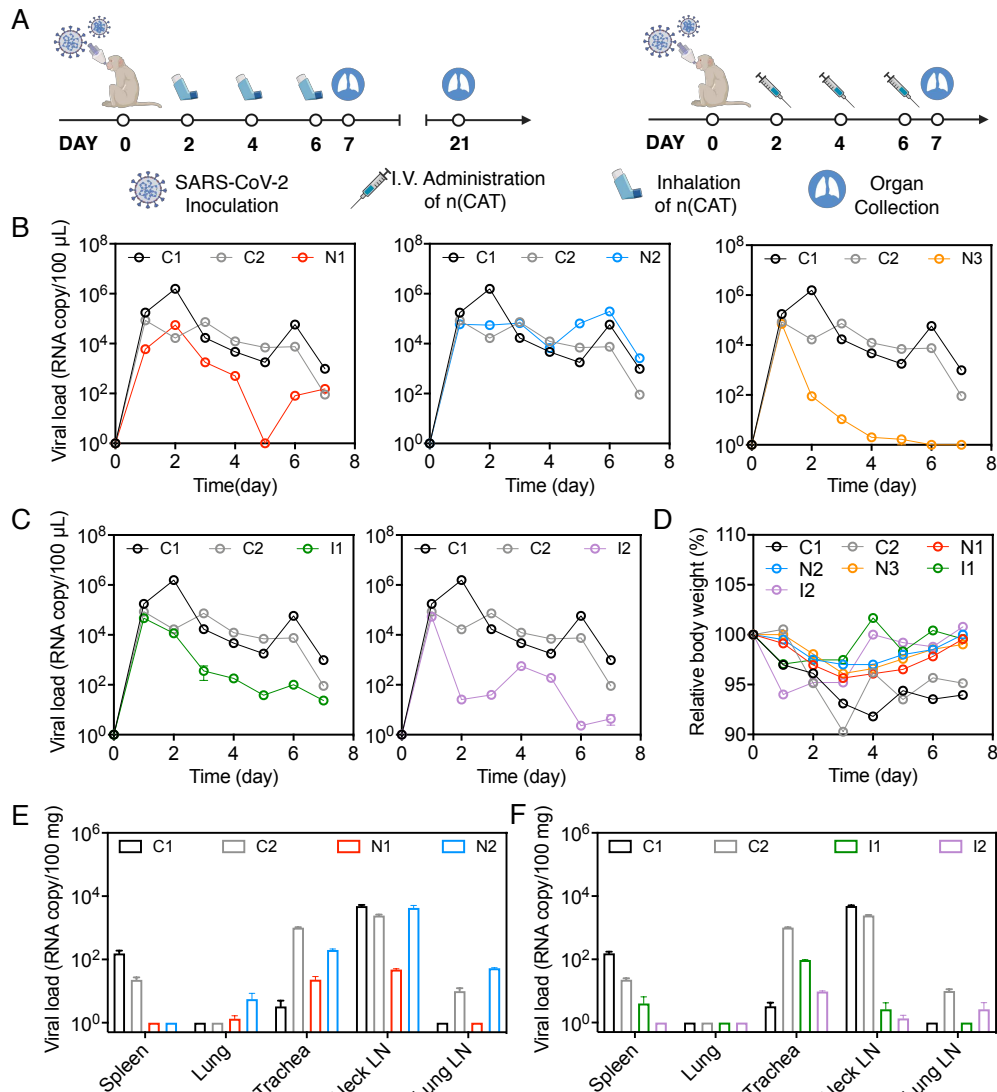
341 **Fig. 1. Characteristic, anti-inflammatory effect, and protective ability of n(CAT).** (A) 342 Dynamic light scattering; (B) zeta potential; (D) thermal stability; (E) proteolytic stability of native 343 catalase and n(CAT). (C) Transmission electron microscopic (TEM) image of n(CAT). (F) Cell 344 viability of HPAEpiC pre-cultured with 20  $\mu$ g/mL n(CAT) for 12 h, followed by addition of  $\text{H}_2\text{O}_2$  345 (1000  $\mu$ M) and culturing for 24 h. (G) Cell viability of HPAEpiC pre-cultured with 1000  $\mu$ M  $\text{H}_2\text{O}_2$  346 for 24 h, followed by culturing in fresh media containing 20  $\mu$ g/ml n(CAT) for 12 h. (H, I) Concentration of (H) TNF- $\alpha$  and (I) IL-10 in the media of human leukocytes (white blood cells, 347 WBC) cultured with LPS and different concentrations of n(CAT). (J) Cell viability of HPAEpiC 348 pre-cultured with 500  $\mu$ M  $\text{H}_2\text{O}_2$  for 12 h (Control #1) followed by culturing with WBC and 349 different concentrations of n(CAT), as well as that of untreated HPAEpiC cultured with WBC for 350 12 h (Control #2). (K) Cell viability of HPAEpiC cultured with LPS (Control #3), with WBC 351 (Control 4#), and with LPS, WBC, and different concentrations of n(CAT).  $P$  value: \*  $< 0.05$ ; \*\* 352  $< 0.01$ ; \*\*\*  $< 0.001$ ; \*\*\*\*  $< 0.0001$ .



354

**Fig. 2. Pharmacokinetics and biodistribution of n(CAT) in mice.** (A) Fluorescence imaging of the major organs, and (B) average radiance of n(CAT) in the liver, lung, and kidney 6 h and 24 h after intravenous administration of 20 mg/kg Cy7-labeled n(CAT). From left to right: heart, liver, spleen, lung, kidney, and lymph nodes. (C) Pharmacokinetics of native catalase and n(CAT) in BALB/c mice ( $n = 3$ ) after intravenous administration of 20 mg/kg native catalase or n(CAT); blood samples were collected 0.1, 1, 3, 6, and 24 h after injection. (D) Drug exposure of the native catalase and n(CAT). (E) Fluorescence imaging of the major organs after intratracheal nebulization of native catalase and n(CAT). From left to right: heart, liver, spleen, lung, and kidney. (F) Relative fluorescence intensity of the lung 48 h after intratracheal nebulization of native catalase and n(CAT).  $P$  value: \*  $< 0.05$ ; \*\*\*\*  $< 0.0001$ .

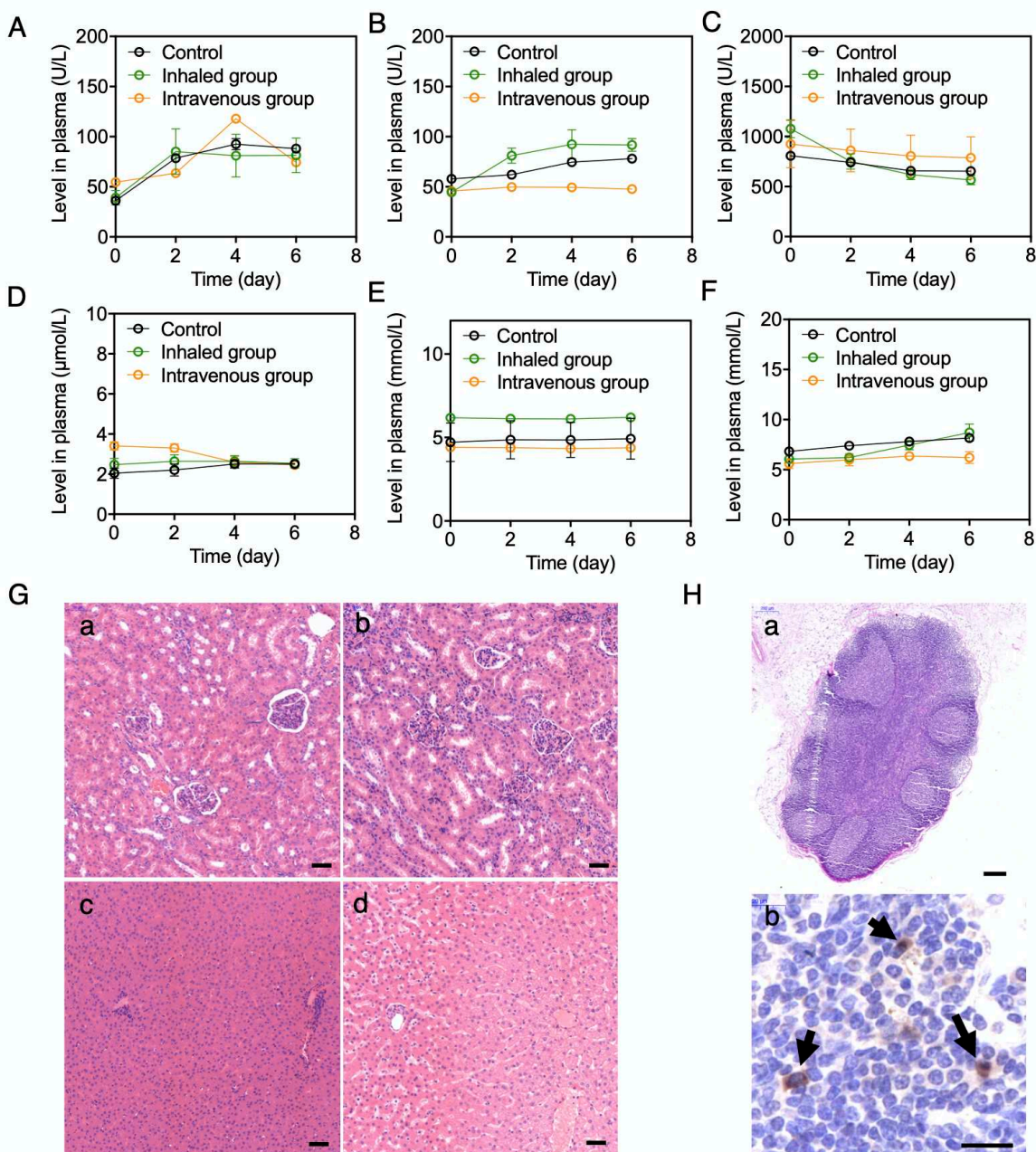
365



366

367 **Fig. 3. Ability of n(CAT) to repress the replication of SARS-CoV-2 in *rhesus macaques*.** (A) 368 Schematic showing the experiment design. (B, C) Viral loads in the nasal swabs of the animals 369 that received (B) nebulization treatment (N1, N2, and N3) and (C) intravenous injection (I1 and 370 I2) of n(CAT). (D) Relative bodyweight of the animals at day 1-7. (E, F) Viral loads in selective 371 organs of the animals receiving (E) nebulization treatment and (F) intravenous injection of n(CAT) 372 at day 7. Animals in the control group were marked as C1 and C2.

373



374

375 **Fig. 4. Biosafety and histology of SARS-CoV-2 infected rhesus macaques.** (A) Aspartate  
376 aminotransferase (AST), (B) alanine aminotransferase (ALT), (C) alkaline phosphatase (ALP), (D)  
377 uric acid (UA), (E) urea, and (F) blood urea nitrogen (BUN) levels of the animals in the control,  
378 inhaled, and intravenous groups. (G) H&E stained sections of the kidneys (a, b) and livers (c, d)  
379 in the control (a, c) and inhaled groups (b, d) (scale bar = 50  $\mu\text{m}$ ). (H) (a) Representative H&E  
380 stained section (scale bar = 200  $\mu\text{m}$ ) and (b) immunohistochemistry staining of SARS-CoV-2  
381 nucleocapsid protein [6H3], demonstrating scattered positive mononuclear cells (arrows) within  
382 the lung LN in C1 (scale bar = 20  $\mu\text{m}$ ).

383